

**Glacier runoff
increases ocean heat
transport along fjords**

A. J. Sole et al.

Increased glacier runoff enhances the penetration of warm Atlantic water into a large Greenland fjord

A. J. Sole^{1,2}, A. J. Payne³, P. W. Nienow², P. Christoffersen⁴, F. R. Cottier⁵, and M. E. Inall⁵

¹Department of Geography, University of Sheffield, Sheffield, S10 2TN, UK

²School of Geosciences, University of Edinburgh, Drummond Street, Edinburgh, EH8 9XP, UK

³Bristol Glaciology Centre, University of Bristol, Bristol BS8, 1SS, UK

⁴Scott Polar Research Institute, University of Cambridge, Cambridge, CB2 1ER, UK

⁵Scottish Association for Marine Science, Scottish Marine Institute, Oban, Argyll, PA37 1QA, UK

Received: 1 November 2012 – Accepted: 12 November 2012 – Published: 27 November 2012

Correspondence to: A. J. Sole (a.sole@sheffield.ac.uk)

Published by Copernicus Publications on behalf of the European Geosciences Union.

Title Page

Abstract

Introduction

Conclusions

References

Tables

Figures

◀

▶

◀

▶

Back

Close

Full Screen / Esc

Printer-friendly Version

Interactive Discussion



Abstract

The retreat and acceleration of Greenland's marine-terminating outlet glaciers have been linked to ocean warming. However the mechanisms which control the transmission of this warming along fjords towards the glaciers remain poorly understood. The aim of this paper is to elucidate observed changes in water properties in Kangerdlugssuaq Fjord (KF), East Greenland using the Bergen Ocean Model (BOM). Model outputs are compared with observed potential temperature, salinity and velocity data to determine the principal controls on heat transport within KF and to estimate resulting submarine ice front melt rates of Kangerdlugssuaq Glacier (KG). The BOM includes wind, tidal and glacier runoff forcing and is able to replicate observed temperature and salinity profiles. Model results describe a robust four-layer estuarine flow, consisting of two distinct circulations. The shallow circulation (0–~60 m) is forced by surface wind stress and to a lesser extent supraglacial runoff, while the intermediate circulation (~60–500 m) is driven by runoff discharged into the fjord subglacially. Atlantic Water (AW) and warm Polar Surface Water (PSWw) are drawn into the fjord by the intermediate and shallow circulation cells respectively, in a pattern consistent with observations, and AW reaches KG over a single summer. Along-fjord heat transport towards KG increases significantly with both glacier runoff and coastal water temperature. A doubling of glacier runoff produces a 29% (48%) amplification of mean annual (summer) heat transport towards the KG terminus, increasing estimated mean annual (summer) submarine melt rates from 211 to 273 (842 to 1244) myr^{-1} . In contrast, heat transport towards KG in the surface ~60 m of the fjord decreases with rising glacier runoff because the enhanced down-fjord component of the intermediate circulation interferes with the up-fjord part of the shallow circulation. Thus, as ice sheet runoff increases, KG's dynamic response to oceanic forcing will likely be driven primarily by enhanced submarine ice front melting and consequent undercutting rather than through diminished buttressing from seasonal sea ice and ice mélange. Our model shows, in agreement with observations, that maximum submarine melt rates occur when AW and

Glacier runoff increases ocean heat transport along fjords

A. J. Sole et al.

Title Page

Abstract

Introduction

Conclusions

References

Tables

Figures



Back

Close

Full Screen / Esc

Printer-friendly Version

Interactive Discussion



1990s, with warm coastal water able to enter the fjord freely at its mouth. By comparing model outputs with observed potential temperature, salinity and velocity data from the early 2000s which characterise “warm” conditions, we aim to determine the principal controls on heat transport within KF. Once identified, we will vary these controls in a manner commensurate with predicted Arctic climate change and examine the effects on heat transport along KF and resulting ice front submarine melt rates of Kangerdlugssuaq Glacier (KG), a large marine-terminating outlet glacier which drains into the fjord.

KF is 70 km long, 5 to 10 km wide, 870 m deep near its mouth (Dowdeswell et al., 2010) and lies adjacent to the meeting point of the Irminger Current (IC) and East Greenland Current (EGC) in an important region of the North Atlantic circulation (Fig. 1). Three principal water masses, defined by their temperature and salinity characteristics (Rudels et al., 2002) and derived from the EGC (Sutherland and Pickart, 2008), are found in KF: Atlantic Water (AW), Polar Surface Water (PSW) and deep ambient fjord water (Christoffersen et al., 2012). The relative proportions of each are controlled by synoptic atmospheric pressure and wind conditions and vary from year to year (Christoffersen et al., 2012). Either AW from the Irminger Sea or cooler Recirculated Atlantic Water (RAW) from higher latitudes can be bathymetrically steered into Kangerdlugssuaq Trough (KT) and towards KF depending on the strength of along-shore winds and the position of the Icelandic Low (Christoffersen et al., 2011).

Between 1993 and 2004, PSW and relatively cool RAW from the Nordic Seas, present in KF in 1993, were replaced by AW from the Irminger Sea and warm Polar Surface Water (Rudels et al., 2002, PSWw – derived from sea ice melting on AW) (Christoffersen et al., 2012) resulting in near-surface and deep (320 to 490 m) water temperatures rising by 4 °C and ~ 1 °C, respectively (Christoffersen et al., 2011) (Fig. 2a).

KG, which lies at the head of KF, is the largest outlet glacier on Greenland’s east coast, and drains ~ 51 000 km² (~ 3 % by area) of the ice sheet (Rignot and Kanagaratnam, 2006). Between summer 2004 and spring 2005, KG retreated by 7 km and

Glacier runoff increases ocean heat transport along fjords

A. J. Sole et al.

[Title Page](#)[Abstract](#)[Introduction](#)[Conclusions](#)[References](#)[Tables](#)[Figures](#)[⏪](#)[⏩](#)[◀](#)[▶](#)[Back](#)[Close](#)[Full Screen / Esc](#)[Printer-friendly Version](#)[Interactive Discussion](#)

accelerated from 7.3 km yr^{-1} to 13.9 km yr^{-1} near its terminus (Howat et al., 2007). The timing of these dramatic changes following the intrusion of AW and PSWw into KF, combined with the near-synchronous reaction of many other South East Greenland outlet glaciers (Luckman et al., 2006), suggests a widescale oceanic forcing (Seale et al., 2011), but the chain of events linking coastal ocean to fjord to glacier remains uncertain.

The amount of ocean heat that is available to melt marine-terminating outlet glaciers at the inland margin of a fjord is controlled by cross-shelf water exchange and circulation within the fjord (Cottier et al., 2010). Here we concentrate on the latter. Most Arctic fjords are bounded at their mouths by a sill, often a remnant terminal moraine from a previous glacier advance, which limits the exchange of water masses between the fjord and shelf (Cottier et al., 2010). Typically, such fjords are assumed to comprise three principal water masses: an outflowing fresh surface layer (containing glacier or terrestrial runoff and melt from icebergs), an intermediate inflowing compensatory layer between the surface outflow and sill depth (Farmer and Freeland, 1983), and a deep layer (Cottier et al., 2010). A more complex transient multilayer circulation pattern with freshwater outflow both at the surface and at the stratification maximum, has recently been observed in Sermilik Fjord (Straneo et al., 2011; Sutherland and Straneo, 2012) but not yet in KF.

Warming of water in contact with marine-terminating outlet glaciers enhances submarine basal melting (Mayer et al., 2000) and also encourages undercutting of ice fronts with resulting increases in calving rates (Eijpen et al., 2003), in some cases by up to ten times the mean melt rate (O'Leary and Christoffersen, 2012). Submarine melt rates at several marine-terminating outlet glaciers in West Greenland (Rignot et al., 2010), where ambient conditions are similar to those in KF, show that rates of up to $\sim 4 \text{ m d}^{-1}$ are possible in summer. This is approximately two orders of magnitude larger than typical subaerial melt rates indicating that submarine melting can play a significant role in marine-terminating glacier mass balance (Christoffersen et al., 2011; Motyka et al., 2003; Rignot et al., 2010). Furthermore, warming of surface waters also

Glacier runoff increases ocean heat transport along fjords

A. J. Sole et al.

Title Page

Abstract

Introduction

Conclusions

References

Tables

Figures

◀

▶

◀

▶

Back

Close

Full Screen / Esc

Printer-friendly Version

Interactive Discussion



reduces the extent and duration of seasonal sea ice and ice mélange cover (a mixture of sea ice and recently calved glacier ice, Sohn et al., 1998) which may in turn diminish buttressing forces at the ice front and thus affect ice flow (Amundson et al., 2010; Christoffersen et al., 2012; Joughin et al., 2008; Nick et al., 2009).

2 Model description

The Bergen Ocean Model (BOM) is a numerical σ -coordinate (bathymetry following) ocean model based on the continuity equation for an incompressible fluid, the Reynolds averaged momentum equations, conservation equations for temperature and salinity and the UNESCO equation of state (Berntsen, 2004). The BOM employs mode splitting (Blumberg and Mellor, 1987) to separate vertically integrated equations and vertical structure equations and solves for the barotropic field (2-D) at higher resolution in time than the baroclinic field (3-D). The model assumes Boussinesq and hydrostatic approximations and has been used previously in many studies of fjord circulation (e.g. Avlesen et al., 2002; Berntsen et al., 2002; Cottier et al., 2005), but has not been applied to a fjord in Greenland.

The σ -coordinate system prescribes thinner vertical layers principally at the surface, but also at the base of the fjord enabling more realistic representation of glacier runoff entering the fjord subglacially. A detailed model description is presented in Berntsen (2004) and so is not included here.

3 Data and methods

The BOM requires several data sets for boundary and initial conditions. Bathymetry is used to constrain the depth and extent of the fjord, water level, potential temperature and salinity data from immediately outside the fjord are used as boundary conditions at the fjord mouth, while surface wind data drive boundary conditions at the fjord surface.

TCD

6, 4861–4896, 2012

Glacier runoff increases ocean heat transport along fjords

A. J. Sole et al.

Title Page

Abstract

Introduction

Conclusions

References

Tables

Figures

◀

▶

◀

▶

Back

Close

Full Screen / Esc

Printer-friendly Version

Interactive Discussion



Potential temperature and salinity data from within the fjord in 1993 are used as initial conditions, while data from 2004 are compared with model outputs, and a glacier runoff timeseries controls the discharge of freshwater into the fjord.

The bathymetry used in the model (Fig. 2) was collected during cruise JR106b of the RRS James Clark Ross from 30 August to 16 September 2004 (Dowdeswell et al., 2004, 2010), supplemented by digitised data from Syvitski et al. (1996). Close to the terminus of KG, where the ice mélange prevented measurements being taken, bathymetry was estimated using the surface elevation of the KG calving front, the maximum draft of icebergs observed in KF, and calculations based on calving front geometry and iceberg flux, giving a water depth of ~ 450 m (Syvitski et al., 1996).

Five temperature and salinity (CTD) profiles were taken between the 4 and 16 September in 1993 – 5, 8, 12 and 50 km from KG terminus (Fig. 2 main and inset a (blue)) (Asprey et al., 1994; Azetsu-Scott and Tan, 1997; Syvitski et al., 1996). These data are used as initial (“cool”) model conditions. The 2004 CTD data (Fig. 2 main and inset a (red)) were acquired from the 1 to 10 September during the same cruise as the bathymetry data (Dowdeswell et al., 2004). Thirty-one profiles were taken in the fjord and close to the fjord mouth. CTD data from 2004 (“warm” conditions) are compared with model outputs to determine model performance.

Tide gauge data (Fig. 3a) were obtained for Angmagssalik (65.5° N, 37° W – approximately 365 km south west from KF) from the British Oceanographic Data Centre (BODC) for the period 1995 to 1996. The resulting tidal range varies between ~ 3.3 m and ~ 1.5 m for spring and neap tides, respectively. Tidal forcing is imposed as a surface elevation boundary condition at the fjord mouth where u , v and water surface height are updated each timestep as a function of time and the amplitudes and phases of the tidal constituents.

Wind forcing data are derived from six-hourly European Centre for Medium-Range Weather Forecasts Interim Reanalysis (ERA-Interim) (1.5° resolution) horizontal wind components at 10 m elevation for 2004 (Simmons et al., 2007) (Fig. 3b) and linearly interpolated onto the model grid. The prevailing wind direction is down-fjord (katabatic)

Glacier runoff increases ocean heat transport along fjords

A. J. Sole et al.

[Title Page](#)[Abstract](#)[Introduction](#)[Conclusions](#)[References](#)[Tables](#)[Figures](#)[⏪](#)[⏩](#)[◀](#)[▶](#)[Back](#)[Close](#)[Full Screen / Esc](#)[Printer-friendly Version](#)[Interactive Discussion](#)

with a maximum magnitude during the modelled period of $\sim 15 \text{ ms}^{-1}$. Surface wind stress is calculated as a quadratic function of the wind speed (W) for speeds less than 11 ms^{-1} , and a cubic function of the wind speed for speeds greater than 11 ms^{-1} (Berntsen, 2004).

$$\begin{aligned}
 5 \quad W < 11 \text{ ms}^{-1} \quad \tau_x &= 1.2 \times 10^{-3} \rho_a |W_x| W_x \\
 &\quad \tau_y = 1.2 \times 10^{-3} \rho_a |W_y| W_y \\
 W > 11 \text{ ms}^{-1} \quad \tau_x &= 1.2 \times 10^{-3} \rho_a |W_x| W_x |W_x| \\
 &\quad \tau_y = 1.2 \times 10^{-3} \rho_a |W_y| W_y |W_y|.
 \end{aligned} \tag{1}$$

10 Drainage basins for each of the glaciers that calve into KF were obtained from a 1 km resolution ice surface DEM (Bamber et al., 2003) and 14 m resolution Landsat satellite imagery. Modelled runoff (Janssens and Huybrechts, 2000) for 2004 of $\sim 2 \text{ km}^3$, presented in Luckman et al. (2006), was used as total glacier runoff from KG basin with a further $\sim 2 \text{ km}^3 \text{ yr}^{-1}$ for subglacial melting produced by frictional heating (Andrews et al., 1994). A mean 2004 melt season duration of ~ 60 days was derived from Wang et al. (2007) so that glacier runoff rates ($\text{m}^3 \text{ s}^{-1}$) could be estimated. These rates were modified into runoff hydrographs for each glacier basin representing the gradual removal of the winter snowpack with elevation during the melt season and subsequent melting of underlying ice until maximum melt extent is reached (Fig. 3c). This time series gives peak runoff for the KG basin of $\sim 1100 \text{ m}^3 \text{ s}^{-1}$ for KG, which compares favourably with other similar estimates (e.g. Rignot et al., 2010). Air temperature forcing of the fjord water is not included because we focus on the role of inflowing water masses and surface fluxes are unlikely to penetrate very deeply in such a strongly stratified environment with constant surface flow (Straneo et al., 2010). The absolute depth and relative proportion of freshwater discharged into the fjord at each depth can be prescribed, enabling the simulation of simultaneous injection of supraglacial and subglacial runoff.

Glacier runoff increases ocean heat transport along fjords

A. J. Sole et al.

Title Page

Abstract

Introduction

Conclusions

References

Tables

Figures



Back

Close

Full Screen / Esc

Printer-friendly Version

Interactive Discussion



The model does not include either wind stress forcing beyond the fjord or external forcing of across shelf properties, apart from the prescribed 1993 to 2004 (“cool” to “warm”) step change in salinity and temperature. While we acknowledge that this limits the possible external influences on heat transport in the fjord, our aim is to identify and quantify the effect that variations in glacier runoff, tides, winds and coastal water properties could have on heat transport *within* KF.

3.1 Model Boundary and Initial Conditions

The standard KF model domain is 81 km by 48 km with a horizontal resolution of 1 km (Fig. 3d) and 63 σ -layers, producing maximum (at the surface) and minimum (at mid-depth) vertical resolutions of 1.5 and 30 m, respectively.

Initially the model is “spun up” with starting temperature and salinity fields based on a piece-wise linear fit to the mean of the five fjord centreline CTD profiles acquired in 1993 (Fig. 2 main and inset a (blue)) and no external forcing. Coastal water properties are set equal to those just inside the fjord, (CF = 0), there is no tidal forcing (TF = 0), no wind forcing (WF = 0) and no glacier runoff forcing (RF = 0) (Fig. 10, Supplement) (CF0-TF0-WF0-RF0). While we acknowledge that these data represent a snapshot of variable conditions in the fjord, their interpolation produces a reasonably stable density field sufficient for initial conditions. Once modelled volume-averaged kinetic and potential energy reach constant values, we assume that water movement due to density gradients has steadied and a state of dynamic equilibrium has been reached. The resulting fields are then used as initial conditions for subsequent experiments.

The advection of AW and PSWw into the fjord is simulated by allowing a reservoir of “coastal” water characterised by four CTD profiles taken from outside the fjord in 2004 (Fig. 2 main and inset a (red)), to flow through an open boundary at the fjord mouth. This flow of water in and out of the fjord is controlled by a 7 km-wide ($y = 0$ to $y = 7$) Flow Relaxation Scheme Zone (FRSZ) (Martinsen and Engedahl, 1987) (Fig. 3d). In this zone, u , v and w , the velocities in the x , y and z directions respectively, are updated

Glacier runoff increases ocean heat transport along fjords

A. J. Sole et al.

Title Page

Abstract

Introduction

Conclusions

References

Tables

Figures



Back

Close

Full Screen / Esc

Printer-friendly Version

Interactive Discussion



at each time step according to

$$\phi = (1 - \alpha)\phi_{\text{INT}} + \alpha\phi_{\text{EXT}} \quad (2)$$

where ϕ_{INT} contains the unrelaxed values computed by the model from within the fjord, and ϕ_{EXT} is a specified external value (Berntsen et al., 2002). The relaxation parameter α varies linearly from 1 at $y = 0$, to 0 at $y = 7$. For our experiments, the external velocities u_{EXT} , v_{EXT} and w_{EXT} are set to be the mean of modelled u , v and w from $y = 8$, to $y = 10$, i.e. the mean velocities with depth for the three rows of grid cells immediately up-fjord of the FRSZ for each timestep; $u, v, w_{\text{EXT}} = u, v, w_{\text{INT}}$ (Fig. 3d). This allows AW and PSWw to enter the fjord where and when there is up-fjord circulation near the fjord mouth, and interior water to leave the fjord where and when the modelled flow is down-fjord (Berntsen et al., 2002). The boundary conditions for temperature, salinity and other scalar variables depend on the direction of v_{EXT} . If v_{EXT} is positive (inflow), a Dirichlet boundary condition (which specifies the value of the variable) is used, if v_{EXT} is negative (outflow), a Neumann boundary condition (which specifies the value of the derivative of the variable) is used (Berntsen et al., 2002). Free slip conditions are applied on the side walls of the fjord and there is a frictional term for the basal drag based on horizontal velocities and water pressure (Berntsen, 2004).

4 Results

We present a series of experiments which all use the final salinity and temperature fields resulting from the spinup experiment as initial (“cool”) conditions. For each experiment we vary the forcings and compare the model output with four CTD profiles taken along the fjord centreline in 2004 (“warm” conditions) at 7.5 km (Pt. 1), 13.5 km (Pt. 2), 37.5 km (Pt. 3) and 44 km (Pt. 4) from the southern boundary of the model domain (Fig. 2). Each experiment is run for 365 days which is sufficient time for dynamic equilibrium to be established and encompasses the whole 2004 melt season for KG and the smaller glacier basins (Wang et al., 2007). By comparing model outputs with

observed potential temperature, salinity and velocity data from 2004, we can determine the principal controls on heat transport within KF. Once identified, we vary these controls in a manner commensurate with predicted Arctic climate change and examine the effects on heat transport along KF and resulting KG ice front submarine melt rates.

4.1 Standard experiment

The “standard” experiment includes glacier runoff forcing using 2004 values ($RF = 1$), wind forcing using 2004 ERA-Interim wind field ($WF = 1$), tidal forcing ($TF = 1$) and assumes no AW or PSWw at the fjord mouth ($CF0-TF1-WF1-RF1$). In other words, these forcings represent conditions in the fjord in 2004 in the absence of AW or PSWw (i.e. with only RAW and PSW present at the fjord mouth). Establishing this “background state” enables the subsequent impact of AW and PSWw arriving at the fjord mouth to be quantified. For this experiment, the majority (90 %) of freshwater discharge into the fjord is introduced at the base of KG (bottom five σ -layers ~ 10 m at KG ice front) and the remaining 10 % in the surface five σ -layers (~ 6 m at KG ice front). This represents the most likely distribution of the total glacier runoff, since the final 10 km of KG are heavily crevassed and most surface melt in this region and supraglacial runoff from further up-glacier, would quickly find its way to the bed as observed elsewhere (Andersen et al., 2010; Cowan, 1992; Jenkins, 2011; Pfirman and Solheim, 1989; Powell and Molina, 1989; Sole et al., 2011). Furthermore, if a large proportion of the runoff were supraglacial, the size of channel required to transport it would be easily identifiable in satellite imagery. No such channels are visible in 14 m resolution Landsat images of the KG terminus. C_M and C_{M2-D} are set to 5 and 250, respectively. These values give the best balance of agreement with existing velocity observations and low computational noise, and fall within the range of those used elsewhere (Berntsen et al., 2002). Model sensitivity to varying the 3-D and 2-D viscosity coefficients (C_M and C_{M2-D} , respectively) is described in Section 5.

Modelled water flow describes two main along-fjord circulation cells (Fig. 4): “shallow” (0– ~ 40 m depth) and “intermediate” (~ 40 – ~ 400 m depth). Averaging the velocity

over many days effectively removes the tidal (barotropic) signal, leaving the underlying (baroclinic) flow. The shallow circulation cell (Fig. 11 Supplement) consists of relatively fresh (salinity 28–30 psu) surface water (0 to ~ 10 m depth) flowing out of the fjord at between 0.025 and 0.075 ms⁻¹, and a compensatory inflow of coastal water of similar speed from ~ 10 to ~ 40 m depth. In the intermediate cell (Fig. 4), water flows out of the fjord between ~ 40 and ~ 250 m depth, and into the fjord between ~ 250 and ~ 400 m depth. This pattern of velocity with depth is not consistent along the length of the fjord, or through time. When KG runoff is < ~ 500 m³ s⁻¹ (prior to day 210 and after day 240), the shallow cell is moderated by tides, with alternating flow in and out of the fjord. However, rising supraglacial runoff in summer, combined with the predominantly down-fjord winds, overcomes the up-fjord component of tidal flow at the surface creating a consistently down-fjord surface outflow and a steady up-fjord compensatory inflow between ~ 10 and ~ 40 m depth. In contrast, the strength of the intermediate inflow is not substantially influenced by tidal flow, but instead scales with the glacier runoff timeseries. This results in significant seasonal variation with a peak in summer and minimal flow during winter.

Temperature changes with time are related only to vertical mixing near the KG ice front, where buoyant glacier runoff and entrained deep water rise through the fjord to immediately beneath the PSW at the surface, and along the entire length of the fjord between ~ 40 and ~ 250 m where the intermediate outflow moves down-fjord. This type of subsurface outflow occurs when the surface layers are less dense than the mixture of submarine glacier runoff and entrained deep ambient water (Christoffersen et al., 2012; Kaartvedt and Svensden, 1995; Straneo et al., 2011).

4.2 AW and PSWw experiment and comparison with observations

Using the same wind, tide and glacier runoff forcing as the standard experiment but with AW and PSWw present at the fjord mouth (CF1-TF1-WF1-RF1) produces a good fit across points 1–4 (mean $r = 0.62$, mean RMSE = 0.72 °C) between modelled temperature profiles and observations (Fig. 5a–d). The correlation between modelled and

Glacier runoff increases ocean heat transport along fjords

A. J. Sole et al.

Title Page

Abstract

Introduction

Conclusions

References

Tables

Figures

◀

▶

◀

▶

Back

Close

Full Screen / Esc

Printer-friendly Version

Interactive Discussion



observed salinity is also good ($r = 0.98$), with RMSE of 0.5. CF = 1 is the difference between the mean fjord temperature and salinity profiles in 1993, and the FRSZ temperature and salinity profiles from 2004 (Fig. 10 Supplement).

Although circulation is comparable to the standard experiment, with two along-fjord circulation cells at similar depths, the modelled temperature and salinity fields along the fjord centre-line reveal significant differences (Fig. 6 and 12 Supplement). Both circulation cells draw coastal water into the fjord, resulting in a AW intrusion from ~ 250 to ~ 500 m and a PSWw intrusion from ~ 0 to ~ 60 m depth. The up-fjord progression of this AW and PSWw corresponds to the circulation described for the standard experiment: the shallow PSWw is influenced by tides resulting in a pulsating advance which becomes predominantly up-fjord as glacier runoff increases, while the intermediate AW intrusion follows the pattern of simulated glacier runoff. After 240 days, the shallow intrusion has increased temperature by $> 2^\circ\text{C}$ from the mouth to approximately 65 km along the fjord, while the intermediate intrusion has produced warming of $\sim 0.5^\circ\text{C}$ and has reached the KG ice front.

By turning on (forcing = 1) and off (forcing = 0) the various forcings (Fig. 5a–d), the principal controls on the influxes of AW and PSWw can be identified. The shallow intrusion (PSWw) is simulated most successfully when surface wind forcing is included (i.e. WF = 1), while the intermediate (AW) intrusion is best captured by experiments involving glacier runoff forcing (i.e. RF = 1) (Table 1). Tidal forcing has little influence on the general circulation and consequent temperature and salinity profiles as it effectively transports water properties backwards and forwards over distances of several kilometres (Straneo et al., 2011).

Water velocity measurements within the fjord are limited to a single transverse section close to the fjord mouth (Sect. 3 – Fig. 2) gathered by Autosub ADCP in 2004 (Dowdeswell et al., 2008), and several measurements from CTD stations within the fjord with average values from 100 to 500 m depth. A comparison between measured (Fig. 5e) and modelled standard (Fig. 5f; mean of days 230 to 240) velocities through Sect. 3 shows that the general pattern of observed flow is captured reasonably well,

Glacier runoff increases ocean heat transport along fjords

A. J. Sole et al.

Title Page

Abstract

Introduction

Conclusions

References

Tables

Figures

◀

▶

◀

▶

Back

Close

Full Screen / Esc

Printer-friendly Version

Interactive Discussion



although modelled velocities are consistently too low. The principal observed inflow is between ~ 300 and ~ 400 m depth, while the main modelled inflow is between ~ 250 and ~ 400 m. The major observed outflow is from ~ 200 to ~ 300 m depth as opposed to ~ 100 to ~ 200 m depth in the model (i.e. modelled intermediate circulation cell). Between the surface and ~ 60 m depth (modelled shallow circulation cell) there is a secondary outflow (0 to ~ 10 m) and inflow (~ 10 to ~ 60 m) in both the modelled and observed velocity data.

4.3 Along-fjord heat transport and submarine ice melt rates

To investigate the potential effects on KG of variations in glacier runoff and coastal water properties, we examined along-fjord heat transport, Q , calculated as follows (Johnson et al., 2011),

$$Q = \int_A \rho_0 c_p (T - T_f) \mathbf{U}_{af} dA \quad (3)$$

where A is cross-sectional area, ρ_0 is the modelled water density (kg m^{-3}), c_p is the specific heat capacity of water ($3986 \text{ J kg}^{-1} \text{ K}^{-1}$), \mathbf{U}_{af} (m s^{-1}) is the along-fjord component of the modelled velocity, and T_f ($^{\circ}\text{C}$) is the local freezing point, based on modelled salinity and pressure.

Q is effectively a measure of the amount of heat available for melting ice (Johnson et al., 2011) and is a preferable metric to water temperature alone because it also contains information on the rate of water flow. Only glacier runoff and coastal water properties (RF and CF, respectively) are varied since it is difficult to envisage a scenario under which tidal and wind forcing would change systematically.

Heat transport is converted to a timeseries of volumetric ice melt rate assuming a latent heat of fusion of $3.3 \times 10^5 \text{ J kg}^{-1}$, an ice density of 930 kg m^{-3} , ice temperature of -10°C and a specific heat of ice of $2100 \text{ J kg}^{-1} \text{ K}^{-1}$ (Sutherland and Straneo, 2012). From this an equivalent ice front melt rate, based on the dimensions of the

Glacier runoff increases ocean heat transport along fjords

A. J. Sole et al.

Title Page

Abstract

Introduction

Conclusions

References

Tables

Figures



Back

Close

Full Screen / Esc

Printer-friendly Version

Interactive Discussion



KG calving front, is derived. This calculation is a minimum estimate of submarine melt rates at KG because it does not include the effect on melting of water flow across the ice front (buoyant and forced convection caused by ice melt and subglacial runoff, respectively; Motyka et al., 2003; White et al., 1980) which will significantly increase melting (Jenkins, 2011). Heat transport and melt rate are calculated for experiments where CF, RF = 0, 0.25, 0.5, 1, 2, 3, 4 (Fig. 10 Supplement). Heat transport through Sect. 2, and corresponding submarine ice front melt rate are shown for these experiments in Fig. 7.

Modelled mean annual (summer: day 180–240) net along-fjord heat transport through Sect. 2 is 7.4×10^9 W (3×10^9 W) directed towards KG for the experiment with AW and PSWw at the fjord mouth. This produces a mean annual (summer) KG ice front melt rate of 211 myr^{-1} (842 myr^{-1}). Heat transport and melt rates show considerable seasonal variability, with mean summer values approximately four times the annual average. This reflects the simulated timeseries of glacier runoff (Fig. 3c) and the consequent strength of the intermediate AW inflow (Fig. 6c). Our modelled heat transport and melt rates are broadly comparable with estimates based on observations from other Greenland fjords (Rignot et al., 2010; Sutherland and Straneo, 2012).

Increasing either RF or CF enhances along-fjord heat transport and consequently ice front melt rate (Fig. 7a, b). Doubling the glacier runoff (RF = 2) leads to a 29% increase (to 273 myr^{-1}) in annual melt rate and a 48% increase (to 1244 myr^{-1}) in summer melt rate, while doubling the water property forcing at the fjord mouth (CF = 2) results in a 75% rise in annual melt rate and a 62% rise in summer melt rate. At higher multiples of standard forcing, increases in RF become more significant than those in CF. This switch occurs because along-fjord water flow continues to strengthen as a result of increased glacier runoff enabling ever more AW and PSWw to reach KG, while only a limited proportion of these waters reaches KG without a concurrent increase in glacier runoff. For example, with AW and PSWw present at the fjord mouth, but with RF = 0.5 and 0.25, mean annual melt rates fall by 27 and 41%, respectively. Maximum submarine melt rates thus occur when AW and PSWw are present at the fjord mouth and, crucially, glacier runoff is also high.

Glacier runoff increases ocean heat transport along fjords

A. J. Sole et al.

[Title Page](#)[Abstract](#)[Introduction](#)[Conclusions](#)[References](#)[Tables](#)[Figures](#)[◀](#)[▶](#)[◀](#)[▶](#)[Back](#)[Close](#)[Full Screen / Esc](#)[Printer-friendly Version](#)[Interactive Discussion](#)

Heat transport between 60 and 500 m (intermediate – Fig. 7c, d) is even more sensitive to glacier runoff, with a twofold rise in the latter leading to annual and summer increases of 58 % and 76 % respectively in the former. In contrast, mean annual and (particularly) summer heat transport towards KG in the top ~ 60 m of the fjord (shallow – Fig. 7e, f) actually decreases as glacier runoff rises. This occurs because the mixture of buoyant glacier runoff and entrained fjord water ascends further through the water column before flowing down fjord and interferes with the upfjord part of the shallow circulation, limiting the intrusion of PSWw. Similarly, heat transport and melt rate are also reduced when coastal water property forcing is increased (Fig. 7e, f). In this case the surface 100 m of the fjord becomes relatively more dense than in the standard experiment because the inflowing coastal water is significantly more salty. As a result, this surface layer is more dense than the rising mixture of glacier runoff and entrained deep water which consequently reaches the surface before flowing down fjord, reversing the shallow PSWw intrusion as it does so. This effect may be muted in reality due to increased melting of icebergs in the surface and subsurface layers of the fjord which is not included in the model.

5 Model sensitivity analysis

We investigate the influence of parameter uncertainty on our model results by conducting a set of experiments in which horizontal grid size, the 3-D (C_M) and 2-D (C_{M2-D}) viscosity coefficients, and the number of vertical layers are individually altered in turn. The effect on along-fjord heat flux of varying each parameter from approximately half to double their standard values is summarized in Fig. 8. The four layer estuarine circulation described above occurred in all the sensitivity experiments indicating it is a robust feature of water flow in KF.

Daily mean heat transport shows a slight monotonic decrease with larger values of C_M and C_{M2-D} (Fig. 8a) which is broadly consistent across experiments where RF was varied (Fig. 8b). This is because along-fjord flows, including the penetration of

Glacier runoff increases ocean heat transport along fjords

A. J. Sole et al.

Title Page

Abstract

Introduction

Conclusions

References

Tables

Figures



Back

Close

Full Screen / Esc

Printer-friendly Version

Interactive Discussion



Glacier runoff increases ocean heat transport along fjords

A. J. Sole et al.

Title Page

Abstract

Introduction

Conclusions

References

Tables

Figures

◀

▶

◀

▶

Back

Close

Full Screen / Esc

Printer-friendly Version

Interactive Discussion



AW and PSWw, tend to be subdued with higher values of C_M and C_{M2-D} . Modelled heat transport is relatively insensitive to the number of vertical layers in the model. Doubling the number of vertical layers results in an increase in heat transport of 12 %, while halving the same parameter leads to a 3 % rise. Increasing the number of vertical layers enables more precise representation of water circulation, principally near the fjord surface and base, but doubles the required computer resources.

Altering horizontal grid size from the standard 1 km to 0.5 km and 1.5 km increases heat flux by 21 and 18 %, respectively. However, at 1.5 km grid size, along fjord flow is not properly represented since in some places the fjord is only two or three cells across. Although using the 0.5 km grid enables higher resolution simulation of water flow, the overall spatial pattern is almost identical to the 1 km experiments and we do not believe the extra computer time required is justified.

6 Discussion

Along-shore surface winds can control water exchange in the top several hundred metres of a fjord by creating a barotropic pressure gradient which drives an intermediate circulation between the fjord and continental shelf (Caceres et al., 2002; Straneo et al., 2010). Although we find that surface winds enhance shallow circulation in KF, wind forcing is not required to propagate the intermediate AW intrusion to the KG ice front within the 365-day model period. This means that the commonly observed estuarine fjord circulation alone can explain the exposure of KG to warm AW and that intermediary circulation, as observed in Sermilik Fjord after storms (Straneo et al., 2010), may not be required. The latter could, however, greatly increase circulation in the fjord, but this remains to be confirmed. We suggest that external forcings, such as synoptic pressure gradients (Christoffersen et al., 2011) and along-shore winds (Straneo et al., 2010), dictate which water masses are present at KF mouth and then circulation driven by glacier runoff is principally responsible for controlling the transport of these waters along the fjord.

Glacier runoff increases ocean heat transport along fjords

A. J. Sole et al.

Title Page

Abstract

Introduction

Conclusions

References

Tables

Figures



Back

Close

Full Screen / Esc

Printer-friendly Version

Interactive Discussion



The modelled inflow of AW is approximately at the KG grounding line depth, so it has the potential to increase calving rate via undercutting of the ice front (Jenkins, 2011; O'Leary and Christoffersen, 2012). Recent modelling has shown that this enhancement can be up to ten times the mean melt rate in cases where melting occurs preferentially at the glacier base (O'Leary and Christoffersen, 2012). Our results show that heat transport towards KG is enhanced by increasing glacier runoff as well as by amplifying the temperature forcing at the fjord mouth which both in turn lead to greater ice front melt rates. Enhanced glacier runoff therefore amplifies submarine ice melt in two complimentary ways; by increasing convection-driven melting at the ice front (Jenkins, 2011), but also by intensifying along-fjord circulation and thus increasing heat transport towards glaciers. Because increasing either glacier runoff or coastal water property forcing reduces the strength of the shallow PSWw intrusion, the dynamic response of KG (and other GrIS outlet glaciers) to oceanic forcing will likely be driven primarily by enhanced submarine ice front melting and consequent undercutting rather than through diminished buttressing from seasonal sea ice and ice mélange.

7 Summary and conclusions

Our model results indicate that a four-layer flow pattern operates in KF (Fig. 9) which is more complex than the simple two-layer estuarine system typically assumed for glaciated fjords. In our model this circulation pattern is caused by a combination of surface winds and the simultaneous injection of glacier runoff into the fjord at the surface and base of marine-terminating outlet glaciers.

There are two distinct along-fjord circulation cells. The “shallow” circulation is limited to the top ~ 60 m of the fjord and is driven by surface winds and supraglacial runoff, while the “intermediate” circulation extends from ~ 60 to ~ 500 m and is controlled by glacier runoff discharged into the fjord subglacially. This circulation pattern produces compensatory inflow of PSWw from ~ 10 to ~ 60 m (shallow) and AW from ~ 250 to ~ 500 m (intermediate) and offers an explanation for warm layers observed at similar

depths in KF in 2004 (Christoffersen et al., 2011). Recent observations from Sermilik Fjord (Straneo et al., 2011; Sutherland and Straneo, 2012) identify a similar multilayer circulation. The AW intrusion reaches the KG terminus over a single melt season. The strength of the intermediate circulation varies significantly over the 365 day model period in accordance with the simulated glacier runoff into the fjord, with a summer peak and minimal flow during winter. Along-fjord heat transport increases significantly with enhanced glacier runoff and ocean temperatures. Doubling glacier runoff produces a 29 % (48 %) amplification of mean annual (summer) heat transport towards the KG terminus, increasing estimated mean annual (summer) submarine melt rates from 211 to 273 (842 to 1244) myr^{-1} . In contrast, heat transport towards KG in the top ~ 60 m of the fjord decreases both when glacier runoff and coastal water temperatures are increased because in each case the enhanced down-fjord component of the intermediate circulation interferes with the up-fjord component of the shallow circulation. Thus, as ice sheet runoff increases, the dynamic response of KG (and other GrIS outlet glaciers) to oceanic forcing will likely be driven primarily by enhanced submarine ice front melting and consequent undercutting rather than through diminished buttressing from seasonal sea ice and ice mélange.

Our model results show, in agreement with observations (Christoffersen et al., 2012), that maximum submarine melt rates occur when AW and PSWw are present at the fjord mouth and, crucially, glacier runoff is also high. This result is consistent with the retreat of KG in 2004–2005 as a major peak in oceanic shoreward heat transport occurred one year earlier (Christoffersen et al., 2011). Enhanced ice sheet runoff therefore increases the sensitivity of KG (and other Greenland marine-terminating glaciers) to ocean warming. The positive relationship between along-fjord heat transport, submarine melting and glacier runoff could initiate a feedback whereby in a high melt year, increased heat transport would enhance submarine ice melt and calving (Jenkins, 2011; O’Leary and Christoffersen, 2012), leading to ice acceleration (Nick et al., 2009), increased dynamic thinning and higher subaerial and basal ice melt rates and runoff (Christoffersen et al.,

Glacier runoff increases ocean heat transport along fjords

A. J. Sole et al.

Title Page

Abstract

Introduction

Conclusions

References

Tables

Figures

◀

▶

◀

▶

Back

Close

Full Screen / Esc

Printer-friendly Version

Interactive Discussion



2012). This feedback would exacerbate Greenland ice loss and could have significant implications for GrIS mass balance.

Supplementary material related to this article is available online at:
<http://www.the-cryosphere-discuss.net/6/4861/2012/tcd-6-4861-2012-supplement.pdf>.

Acknowledgements. The authors would like to thank Julian Dowdeswell and Karen Heywood for kindly providing the Kangerdlugssuaq Fjord bathymetry and temperature and salinity data respectively, and Jarle Berntsen and the other Bergen Ocean Model authors for making their code freely available. The temperature and salinity data collection, quality control and processing were funded by the UK Natural Environmental Research Council (NERC) (NER/T/S/2000/0099). The bathymetry data collection was supported by NERC's Autosub Under Ice Thematic Programme. Contributions from MEI and FRC were supported by NERC (NE/I017704/1) and AS by NERC (NE/F021399/1) to PN.

References

- Amundson, J., Fahnestock, M., Truffer, M., Brown, J., Lu thi, M., and Motyka, R.: Ice melange dynamics and implications for terminus stability, Jakobshavn Isbræ, Greenland, *J. Geophys. Res.*, 115, F01005, doi:10.1029/2009JF001405, 2010. 4866
- Andersen, M., Larsen, T., Nettles, M., Elosegui, P., van As, D., Hamilton, G., Stearns, L., Davis, J., Ahlstrom, A., de Juan, J., Ekstrom, G., Stenseng, L., Khan, S., Forsberg, R., and Dahl-Jensen, D.: Spatial and temporal melt variability at Helheim Glacier, East Greenland, and its effect on ice dynamics, *J. Geophys. Res.*, 115, F04041, doi:10.1029/2010JF001760, 2010. 4871
- Andrews, J. T., Milliman, J. D., Jennings, A. E., Rynes, N., and Dwyer, J.: Sediment thicknesses and Holocene glacial marine sedimentation rates in three East Greenland fjords (ca. 68° N), *J. Geol. Today*, 102, 669–683, 1994. 4868

Glacier runoff increases ocean heat transport along fjords

A. J. Sole et al.

Title Page

Abstract

Introduction

Conclusions

References

Tables

Figures



Back

Close

Full Screen / Esc

Printer-friendly Version

Interactive Discussion



**Glacier runoff
increases ocean heat
transport along fjords**A. J. Sole et al.

[Title Page](#)[Abstract](#)[Introduction](#)[Conclusions](#)[References](#)[Tables](#)[Figures](#)[◀](#)[▶](#)[◀](#)[▶](#)[Back](#)[Close](#)[Full Screen / Esc](#)[Printer-friendly Version](#)[Interactive Discussion](#)

Asprey, K., Syvitski, J., Andrews, J., and Dowdeswell, J.: CANAM-PONAM Cruise HU93030: West Iceland to East Greenland, Geological Survey of Canada, Open File Report 2824, 1994. 4867

Avlesen, H., Berntsen, J., and Furnes, G.: On the current conditions along the Ormen Lange pipeline path during an extreme, idealized storm passage, Tech. rep., Department of Informatics, University of Bergen, 2002. 4866

Azetsu-Scott, K. and Tan, F.: Oxygen isotope studies from Iceland to an East Greenland Fjord: behaviour of glacial meltwater plume, *Mar. Chem.*, 56, 239–251, 1997. 4867

Bamber, J., Baldwin, D., and Gogineni, P.: A new bedrock and surface elevation dataset for modelling the Greenland ice sheet, *Ann. Glaciol.*, 37, 351–356, 2003. 4868

Berntsen, J.: Users guide for a modesplit sigma-coordinate numerical ocean model, Tech. rep., Institute of Mathematics, University of Bergen, 2004. 4866, 4868, 4870

Berntsen, J., Aksnes, D., and Foldvik, A.: Production enhancement by artificial upwelling: a simulation study, *Hydrobiologia*, 484, 177–190, 2002. 4866, 4870, 4871

Blumberg, A. and Mellor, G.: description of a three-dimensional coastal ocean circulation model, in: *Three-Dimensional Coastal Ocean Models*, American Geophysical Union, 1–16, 1987. 4866

Box, J., Cappelen, J., Chen, C., Decker, D., Fettweis, X., Hall, D., Hanna, E., Jorgensen, B., Knudsen, N., Lipscomb, W., Mernild, S., Mote, T., Steiner, N., Tedesco, M., van de Wal, R., and Wahr, J.: Arctic Report Card 2011: Greenland Ice Sheet, Tech. rep., National Oceanic and Atmospheric Administration, 2011. 4863

Caceres, M., Valle-Levinson, A., Sepulveda, H., and Holderied, K.: Transverse variability of flow and density in a Chilean fjord, *Cont. Shelf Res.*, 22, 1683–1698, 2002. 4877

Christoffersen, P., Mugford, R. I., Heywood, K. J., Joughin, I., Dowdeswell, J. A., Syvitski, J. P. M., Luckman, A., and Benham, T. J.: Warming of waters in an East Greenland fjord prior to glacier retreat: mechanisms and connection to large-scale atmospheric conditions, *The Cryosphere*, 5, 701–714, doi:10.5194/tc-5-701-2011, 2011. 4863, 4864, 4865, 4877, 4879

Christoffersen, P., O'Leary, M., van Angelen, J., and van den Broeke, M.: Partitioning effects from ocean and atmosphere on the calving stability of Kangerdlugssuaq Glacier, East Greenland, *Ann Glaciol.*, 53, 249–256, doi:10.3189/2012AoG60A087, 2012. 4864, 4866, 4872, 4879

Glacier runoff increases ocean heat transport along fjords

A. J. Sole et al.

[Title Page](#)
[Abstract](#)
[Introduction](#)
[Conclusions](#)
[References](#)
[Tables](#)
[Figures](#)
[Back](#)
[Close](#)
[Full Screen / Esc](#)
[Printer-friendly Version](#)
[Interactive Discussion](#)


- Cottier, F., Tverberg, V., Inall, M., Svendsen, H., Nilsen, F., and Griffiths, C.: Water mass modification in an Arctic fjord through cross-shelf exchange: the seasonal hydrography of Kongsfjorden, Svalbard, *J. Geophys. Res.*, 110, C12005, doi:10.1029/2004JC002757, 2005. 4866
- 5 Cottier, F., Nilsen, F., Skogseth, R., Tverberg, V., Skardhamar, J., and Svendsen, H.: Arctic fjords: a review of the oceanographic environment and dominant physical processes, in: *Fjord Systems and Archives*, no. 344 in Geological Society, Special Publications, The Geological Society of London, London, doi:10.1144/SP344.4, 35–50, 2010. 4863, 4865
- Cowan, E.: Meltwater and tidal currents: controls on circulation in a small glacial fjord, *Estuar. Coast. Shelf S.*, 34, 381–392, 1992. 4871
- 10 Dowdeswell, J., Evans, J., O Cofaigh, C., Mugford, R., McPhail, S., Peabody, M., Stevenson, P., Webb, A., White, D., Heywood, K., Price, M., O'Mahoney, P., Sime, L., Clement, P., Dodd, P., Bett, B., Jones, D., Tyler, P., Swift, D., Edwards, T., Cooper, P., Tait, A., and Willis, D.: Cruise report – JR106b RRS James Clark Ross NERC Autosub under ice thematic programme Kangerdlussuaq Fjord and shelf East Greenland, Tech. rep., NERC, 2004. 4867
- 15 Dowdeswell, J., Evans, J., Mugford, R., Griffiths, G., McPhail, S., Millard, N., Stevenson, P., Brandon, M., Banks, C., Heywood, K., Price, M., Dodd, P., Jenkins, A., Nicholls, K., Hayes, D., Abrahamsen, E., Tyler, P., Bett, B., Jones, D., Wadhams, P., Wilkinson, J., Stansfield, K., and Ackley, S.: Autonomous underwater vehicles (AUVs) and investigations of the ice–ocean interface in Antarctic and Arctic waters, *J. Glaciol.*, 54, 661–672, 2008. 4873, 4892
- 20 Dowdeswell, J., Evans, J., and O Cofaigh, C.: Submarine landforms and shallow acoustic stratigraphy of a 400 km-long fjord-shelf-slope transect, Kangerlussuaq margin, East Greenland, *Quaternary Sci. Rev.*, 29, 3359–3369, doi:10.1016/j.quascirev.2010.06.006, 2010. 4864, 4867
- Eijpen, K., Warren, C., and Benn, D.: Subaqueous melt rates at calving termini: a laboratory approach, *Ann. Glaciol.*, 36, 79–183, 2003. 4865
- 25 Farmer, D. and Freeland, H.: The physical oceanography of fjords, *Prog. Oceanogr.*, 12, 147–220, 1983. 4865
- Hanna, E., Cappelen, J., Fettweis, X., Huybrechts, P., Luckman, A., and Ribergaard, M.: Hydrologic response of the Greenland ice sheet: the role of oceanographic warming, *Hydrol. Process.*, 23, 7–30, 2009. 4863
- 30 Hanna, E., Huybrechts, P., Cappelen, J., Steffen, K., Bales, R., Burgess, E., McConnell, J., Stefensen, J., Van den Broeke, M., Wake, L., Bigg, G., Griffiths, M., and Savas, D.: Greenland Ice Sheet surface mass balance 1870 to 2010 based on Twentieth Century Reanalysis, and links

Glacier runoff increases ocean heat transport along fjords

A. J. Sole et al.

[Title Page](#)
[Abstract](#)
[Introduction](#)
[Conclusions](#)
[References](#)
[Tables](#)
[Figures](#)
[Back](#)
[Close](#)
[Full Screen / Esc](#)
[Printer-friendly Version](#)
[Interactive Discussion](#)


with global climate forcing, *J. Geophys. Res.*, 116, D24121, doi:10.1029/2011JD016387, 2011. 4863

Holland, D., Thomas, R., De Young, B., Ribergaard, M., and Lyberth, B.: Acceleration of Jakobshavn Isbae triggered by warm subsurface ocean waters, *Nat. Geosci.*, 1, 659–664, 2008. 4863

Howat, I., Joughin, I., and Scambos, T.: Rapid changes in ice discharge from Greenland outlet glaciers, *Science*, 315, 1559–1561, 2007. 4865

Janssens, I. and Huybrechts, P.: The treatment of meltwater retention in mass-balance parameterizations of the Greenland ice sheet, *Ann. Glaciol.*, 31, 133–140, 2000. 4868

Jenkins, A.: Convection-driven melting near the grounding lines of ice shelves and tidewater glaciers, *J. Phys. Oceanogr.*, 41, 2279–2294, doi:10.1175/JPO-D-11-03.1, 2011. 4871, 4875, 4878, 4879

Johnson, H., Munchow, A., Falkner, K., and Melling, H.: Ocean circulation and properties in Petermann Fjord, Greenland, *J. Geophys. Res.*, 116, C01003, doi:10.1029/2010JC006519, 2011. 4874

Joughin, I., Howat, I., Fahnestock, M., Smith, B., Krabill, W., Alley, R., Stern, H., and Truffer, M.: Continued evolution of Jakobshavn Isbrae following its rapid speedup, *J. Geophys. Res.*, 113, F04006, doi:10.1029/2008JF001023, 2008. 4866

Kaartvedt, S. and Svensden, H.: Effect of freshwater discharge, intrusions of coastal water, and bathymetry on zooplankton distribution in a Norwegian Fjord system, *J. Plankton Res.*, 17, 493–511, 1995. 4872

Luckman, A., Murray, T., de Lange, R., and Hanna, E.: Rapid and synchronous ice-dynamics changes in East Greenland, *Geophys. Res. Lett.*, 33, L03503, doi:10.1029/2005GL022519, 2006. 4865, 4868

Martinsen, E. and Engedahl, H.: Implementation and testing of a lateral boundary scheme as an open boundary condition in a barotropic ocean model, *Coast. Eng.*, 11, 603–627, 1987. 4869

Mayer, C., Reeh, N., Jung-Rothenhausler, H., Huybrechts, P., and Oerter, H.: The subglacial cavity and implied dynamics under Nioghalvfjærdsfjorden Glacier, NE-Greenland, *Geophys. Res. Lett.*, 27, 2289–2292, 2000. 4865

Meehl, G., Stocker, T., Collins, W., Friedlingstein, P., Gaye, A., Greg, J., Kitoh, A., Knutti, R., Murphy, J., Noda, A., Raper, S., Watterson, I., Weaver, A., and Zhao, Z.-C.: Global climate projections, in: *Climate Change 2007: The Physical Science Basis. Contribution of Work-*

Glacier runoff increases ocean heat transport along fjords

A. J. Sole et al.

Title Page

Abstract

Introduction

Conclusions

References

Tables

Figures

◀

▶

◀

▶

Back

Close

Full Screen / Esc

Printer-friendly Version

Interactive Discussion



ing Group I to the Fourth Assessment Report of the Intergovernmental Panel on Climate Change, Cambridge University Press, 747–844, 2007. 4863

Mortensen, J., Lennert, K., Bendtsen, J., and Rysgaard, S.: Heat sources for glacial melt in a sub-Arctic fjord (Godthabsfjord) in contact with the Greenland ice sheet, *J. Geophys. Res.*, 116, C01013, doi:10.1029/2010JC006528, 2011. 4863

Motyka, R., Hunter, L., Echelmeyer, K., and Connor, C.: Submarine melting at the terminus of a temperate tidewater glacier, LeConte Glacier, Alaska, U.S.A., *Ann. Glaciol.*, 36, 57–65, 2003. 4865, 4875

Murray, T., Scharrer, K., James, T., Dye, S., Hanna, E., Booth, A., Selmes, N., Luckman, A., Hughes, A., Cook, S., and Huybrechts, P.: Ocean regulation hypothesis for glacier dynamics in Southeast Greenland and implications for ice sheet mass changes, *J. Geophys. Res.*, 115, F03026, doi:10.1029/2009JF001522, 2010. 4863

Nick, F., Vieli, A., Howat, I., and Joughin, I.: Large-scale changes in Greenland outlet glacier dynamics triggered at the terminus, *Nat. Geosci.*, 2, 110–114, doi:10.1038/NGEO394, 2009. 4863, 4866, 4879

O’Leary, M. and Christoffersen, P.: Calving on tidewater glaciers amplified by submarine frontal melting, *The Cryosphere Discuss.*, 6, 3287–3316, doi:10.5194/tcd-6-3287-2012, 2012. 4865, 4878, 4879

Pfirman, S. and Solheim, A.: Subglacial meltwater discharge in the open-marine tidewater glacier environment: observations from Nordaustlandet, Svalbard Archipelago, *Mar. Geol. Today*, 86, 265–281, 1989. 4871

Powell, R. and Molina, B.: Glacimarine sedimentary processes, facies and morphology of the South-Southeast Alaska shelf and fjords, *Mar. Geol.*, 85, 359–390, 1989. 4871

Pritchard, H., Arthern, R., Vaughan, D., and Edwards, L.: Extensive dynamic thinning on the margins of the Greenland and Antarctic ice sheets, *Nature*, 461, 971–975, doi:10.1038/nature08471, 2009. 4863

Rignot, E. and Kanagaratnam, P.: Changes in the velocity structure of the Greenland ice sheet, *Science*, 311, 986–990, 2006. 4864

Rignot, E., Box, J., Burgess, E., and Hanna, E.: Mass balance of the Greenland ice sheet from 1958 to 2007, *Geophys. Res. Lett.*, 35, L20502, doi:10.1029/2008GL035417, 2008. 4863

Rignot, E., Koppes, M., and Velicogna, I.: Rapid submarine melting of the calving faces of West Greenland glaciers, *Nat. Geosci.*, 3, 187–191, doi:10.1038/NGEO765, 2010. 4865, 4868, 4875

Glacier runoff increases ocean heat transport along fjords

A. J. Sole et al.

[Title Page](#)
[Abstract](#)
[Introduction](#)
[Conclusions](#)
[References](#)
[Tables](#)
[Figures](#)
[Back](#)
[Close](#)
[Full Screen / Esc](#)
[Printer-friendly Version](#)
[Interactive Discussion](#)


- Rignot, E., Velicogna, I., van den Broeke, M., Monaghan, A., and Lenaerts, J.: Acceleration of the contribution of the Greenland and Antarctic ice sheets to sea level rise, *Geophys. Res. Lett.*, 38, L05503, doi:10.1029/2011GL046583, 2011. 4863
- Rudels, B., Fahrbach, E., Meincke, J., Budeus, G., and Eriksson, P.: The East Greenland Current and its contribution to the Denmark Strait overflow, *ICES J. Mar. Sci.*, 59, 1133–1154, 2002. 4864
- Seale, A., Christoffersen, P., Mugford, R., and O’Leary, M.: Ocean forcing of the Greenland Ice Sheet: calving fronts and patterns of retreat identified by automatic satellite monitoring of eastern outlet glaciers, *J. Geophys. Res.*, 116, F03013, doi:10.1029/2010JF001847, 2011. 4863, 4865
- Simmons, A., Uppala, S., Dee, D., and Kobayashi, S.: ERA-Interim: New ECMWF reanalysis products from 1989 onwards, *ECMWF Newsletter*, 110, 2007. 4867
- Sohn, H.-G., Jezek, K., and van de Veen, C.: Jakobshavn Glacier, West Greenland: 30 years of spaceborne observations, *Geophys. Res. Lett.*, 25, 2699–2702, 1998. 4866
- Sole, A., Mair, D., Nienow, P., Bartholomew, I., King, M., and Burke, M.: Seasonal speedup of a Greenland marine-terminating outlet glacier forced by surface melt-induced changes in subglacial hydrology, *J. Geophys. Res.*, 116, F03014, doi:10.1029/2010JF001948, 2011. 4871
- Straneo, F., Hamilton, G., Sutherland, D., Stearns, L., Davidson, F., Hammill, M., Stenson, G., and Rosing-Asvid, A.: Rapid circulation of warm subtropical waters in a major glacial fjord in East Greenland, *Nat. Geosci.*, 3, 182–186, doi:10.1038/ngeo764, 2010. 4863, 4868, 4877
- Straneo, F., Curry, R. G., Sutherland, D. A., Hamilton, G. S., Cenedese, C., Vage, K., and Stearns, L. A.: Impact of fjord dynamics and glacial runoff on the circulation near Helheim Glacier, *Nat. Geosci.*, 4, 322–327, doi:10.1038/ngeo1109, 2011. 4863, 4865, 4872, 4873, 4879
- Sutherland, D. and Pickart, R.: The east greenland coastal current: structure, variability, and forcing, *Prog. Oceanogr.*, 78, 58–77, 2008. 4864
- Sutherland, D. and Straneo, F.: Estimating ocean heat transports and submarine melt rates in Sermilik Fjord, Greenland, using lowered acoustic Doppler current profiler (LADCP) velocity profiles, *Ann. Glaciol.*, 53, 50–58, doi:10.3189/2012AoG60A050, 2012. 4865, 4874, 4875, 4879, 4894

Glacier runoff increases ocean heat transport along fjords

A. J. Sole et al.

[Title Page](#)[Abstract](#)[Introduction](#)[Conclusions](#)[References](#)[Tables](#)[Figures](#)[◀](#)[▶](#)[◀](#)[▶](#)[Back](#)[Close](#)[Full Screen / Esc](#)[Printer-friendly Version](#)[Interactive Discussion](#)

Syvitski, J., Andrews, J., and Dowdeswell, J.: Sediment deposition in an iceberg-dominated glacimarine environment, East Greenland: basin fill implications, *Global Planet. Change*, 12, 251–270, 1996. 4867

5 Tedesco, M., Serreze, M., and Fettweis, X.: Diagnosing the extreme surface melt event over southwestern Greenland in 2007, *The Cryosphere*, 2, 159–166, doi:10.5194/tc-2-159-2008, 2008. 4863

van den Broeke, M., Bamber, J., Ettema, J., Rignot, E., Schrama, E., and van de Berg, W., van Meijgaard, E., Velicogna, I., and Wouters, B.: Partitioning recent Greenland mass loss, *Science*, 326, 984–986, doi:10.1126/science.1178176, 2009. 4863

10 Wang, L., Sharp, M., Rivard, B., and Steffen, K.: Melt season duration and ice layer formation on the Greenland ice sheet, 2000–2004, *J. Geophys. Res.*, 112, F04013, doi:10.1029/2007JF000760, 2007. 4868, 4870

15 White, F., Spaulding, M., and Gominho, L.: Theoretical estimates of the various mechanisms involved in iceberg deterioration in the open ocean environment, University of Rhode Island for United States Coast Guard, Tech. rep., 1980. 4875

Glacier runoff increases ocean heat transport along fjords

A. J. Sole et al.

Table 1. Goodness of fit statistics for model experiments with and without wind forcing (WF) and glacier runoff forcing (RF). “Shallow” = < 60 m, “Intermediate” = > 60 m.

		<i>r</i> shallow		RMSE shallow			<i>r</i> intermediate		RMSE intermediate	
		temp	sal	temp	sal		temp	sal	temp	sal
Pt. 1	WF = 1	0.43	0.89	1.24	0.85	RF = 1	0.87	0.99	0.41	0.16
	WF = 0	0.13	0.95	2.51	0.33	RF = 0	0.72	0.99	0.64	0.14
Pt. 2	WF = 1	0.45	0.91	1.32	1.15	RF = 1	0.88	0.98	0.21	0.17
	WF = 0	0.27	0.98	1.08	0.50	RF = 0	0.72	0.99	0.40	0.13
Pt. 3	WF = 1	0.55	0.94	0.60	0.96	RF = 1	0.86	0.99	0.16	0.13
	WF = 0	-0.62	0.93	0.86	0.30	RF = 0	0.60	0.99	0.46	0.15
Pt. 4	WF = 1	0.10	0.87	1.13	1.05	RF = 1	0.85	0.99	0.18	0.22
	WF = 0	-0.67	0.97	0.70	0.29	RF = 0	0.69	0.99	0.35	0.13

Title Page

Abstract

Introduction

Conclusions

References

Tables

Figures

◀

▶

◀

▶

Back

Close

Full Screen / Esc

Printer-friendly Version

Interactive Discussion



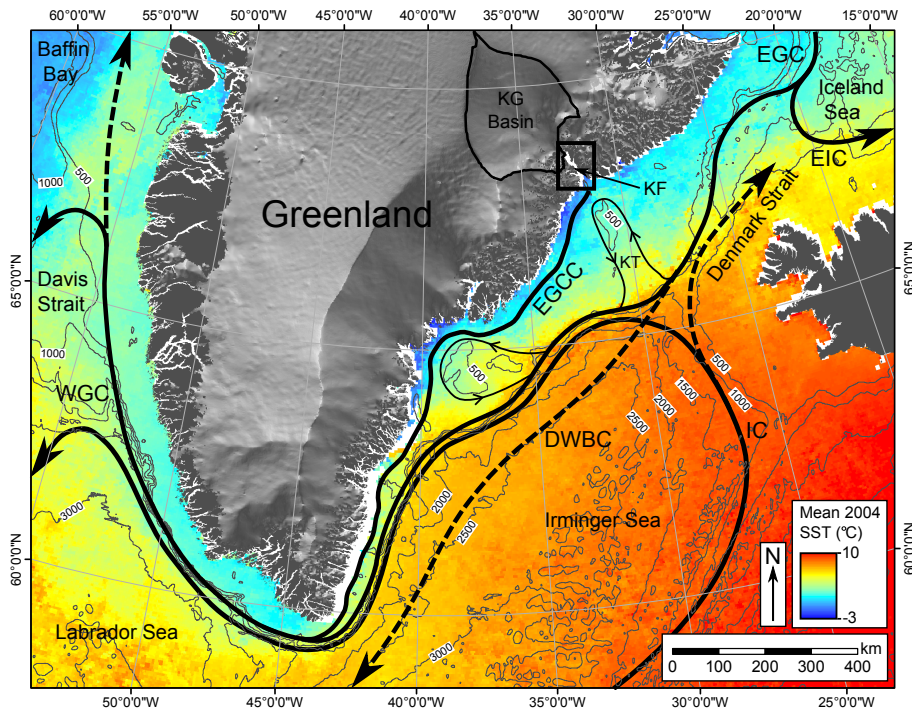


Fig. 1. The sub-polar gyre. Background colour shows mean annual AVHRR 4 km sea surface temperature for 2004. Grey contours (500 m interval) show bathymetry based on data from the Earth Topographic database ETOPO1. Also shown are the principal ocean currents: East Greenland Current (EGC); East Greenland Coastal Current (EGCC); East Iceland Current (EIC); Irminger Current (IC); West Greenland Current (WGC) and the principal deep water current: Deep Western Boundary Current (DWBC). Kangerdlugssuaq Gletscher (KG) Basin, Kangerdlugssuaq Fjord (KF) and Kangerdlugssuaq Trough (KT) are also indicated. The black box delineates the area magnified in Fig. 2.

Glacier runoff increases ocean heat transport along fjords

A. J. Sole et al.

Discussion Paper | Discussion Paper | Discussion Paper | Discussion Paper

Title Page

Abstract Introduction

Conclusions References

Tables Figures

◀ ▶

◀ ▶

Back Close

Full Screen / Esc

Printer-friendly Version

Interactive Discussion



Glacier runoff increases ocean heat transport along fjords

A. J. Sole et al.

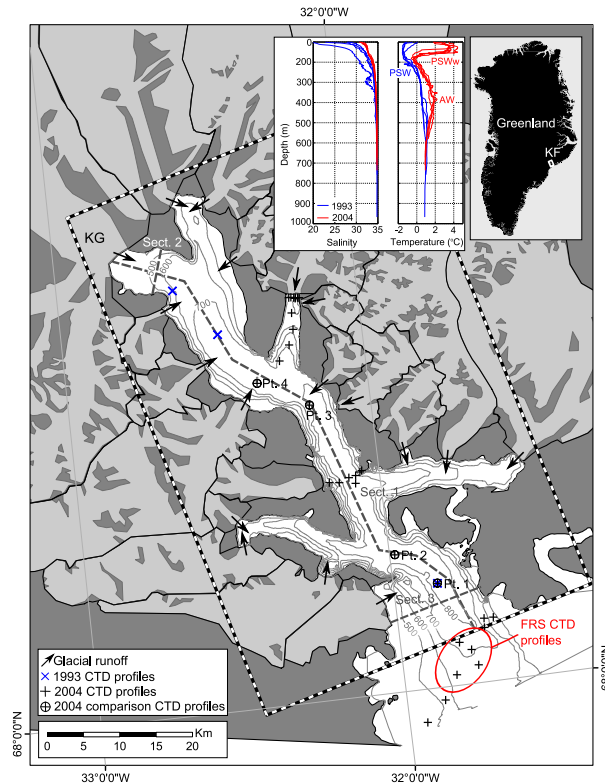


Fig. 2. Kangerdlugssuaq Fjord (KF) showing model domain (black and white box) and CTD profile locations. Also shown are the locations of the along-fjord (Sect. 1) and across-fjord (Sects. 2 and 3) sections (grey dashed lines). Ice covered areas are shown in light grey and ice free areas in dark grey, while ice drainage basins for freshwater inflow estimation are delineated in black. Inset a: a comparison of CTD profiles taken 5, 8, 12 and 50 km from the KG terminus in 1993 (blue) and from the mouth of KF in 2004 (red). See main panel for locations. Inset b: KF location.

Glacier runoff increases ocean heat transport along fjords

A. J. Sole et al.

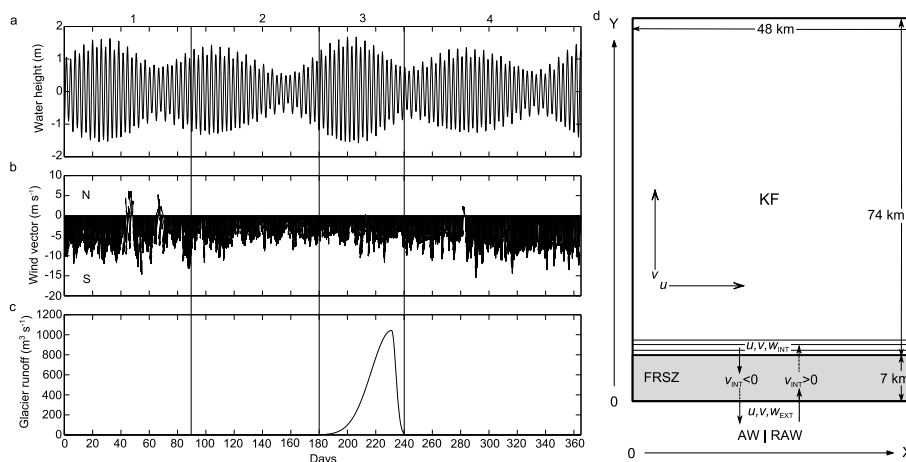


Fig. 3. BOM forcing. **(a)** tidal forcing used to drive water levels in the FRSZ; **(b)** mean surface wind direction and magnitude for the model domain (1 January 2004–31 December 2004); **(c)** modelled glacier runoff for KG basin. The modelled period is split into 4 stages: 1, 0–90 days; 2, 91–180 days; 3, 181–240 days and; 4, 241–365 days. These stages correspond to **(a–d)** in Figs. 6, 7, 9 and 10; **(d)** BOM domain showing boundary conditions at the fjord mouth. The external velocities u_{EXT} , v_{EXT} and w_{EXT} are set to be the mean of modelled u , v and w from $y = 8$, to $y = 10$, i.e. the mean velocities with depth for the three rows of grid cells immediately up-fjord of the FRSZ for each timestep; $u, v, w_{EXT} = u, v, w_{INT}$. This allows AW and PSWw to enter the fjord where and when there is up-fjord circulation near the fjord mouth, and interior water to leave the fjord where and when the modelled flow is down-fjord.

Title Page

Abstract

Introduction

Conclusions

References

Tables

Figures

◀

▶

◀

▶

Back

Close

Full Screen / Esc

Printer-friendly Version

Interactive Discussion



Glacier runoff increases ocean heat transport along fjords

A. J. Sole et al.

Title Page

Abstract

Introduction

Conclusions

References

Tables

Figures

◀

▶

◀

▶

Back

Close

Full Screen / Esc

Printer-friendly Version

Interactive Discussion

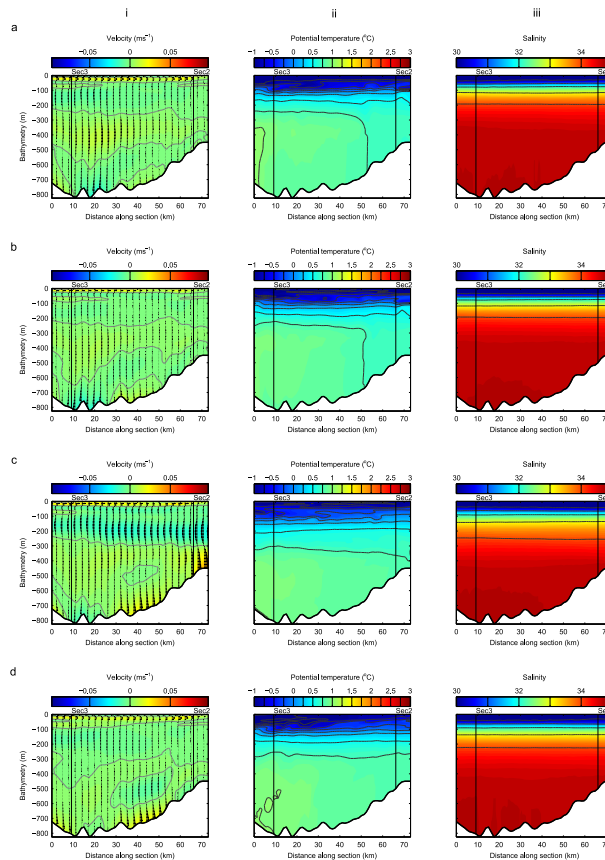


Fig. 4. Longitudinal section (Sect. 1) for experiment CF0-TF1-WF1-RF1. Velocity parallel to Sect. 1 (i), potential temperature (ii) and salinity (iii) for mean of days 0–90 (a), days 91–180 (b), days 181–240 (c) and days 241–365 (d). The fjord mouth is to the left of each plot, and the KG terminus to the right. The FRSZ is not plotted.

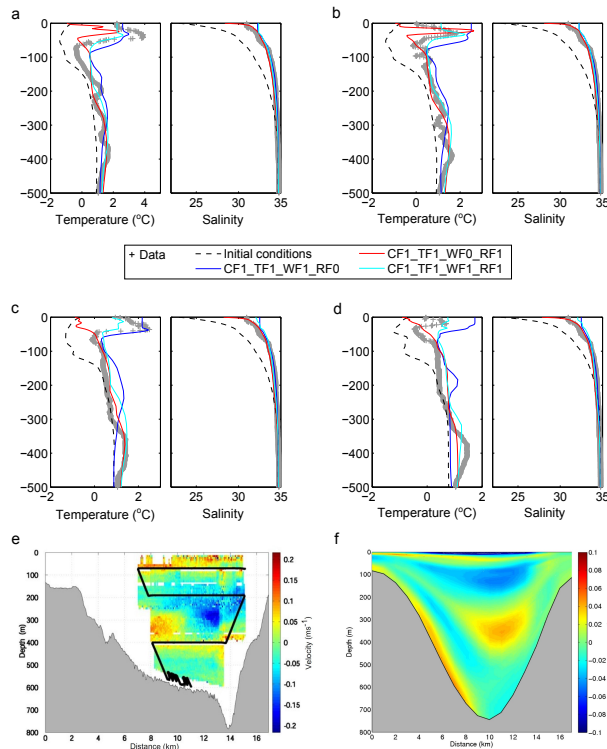


Fig. 5. (a–d) A comparison between observed and modelled temperature and salinity at Points 1 to 4 (a–d – see Fig. 2) highlighting the effect of wind and glacier runoff forcing. CF = coastal anomaly forcing; TF = tidal forcing; WF = wind forcing; RF = glacier runoff forcing. 1 = on; 0 = off; **(e–f)** a comparison of observed **(e)** and modelled **(f)** along-fjord velocities close to the fjord mouth (note different colour scales). Positive values show water flowing into the fjord while negative values show water flowing out of the fjord. **(e)** Is taken from (Dowdeswell et al., 2008).

Glacier runoff increases ocean heat transport along fjords

A. J. Sole et al.

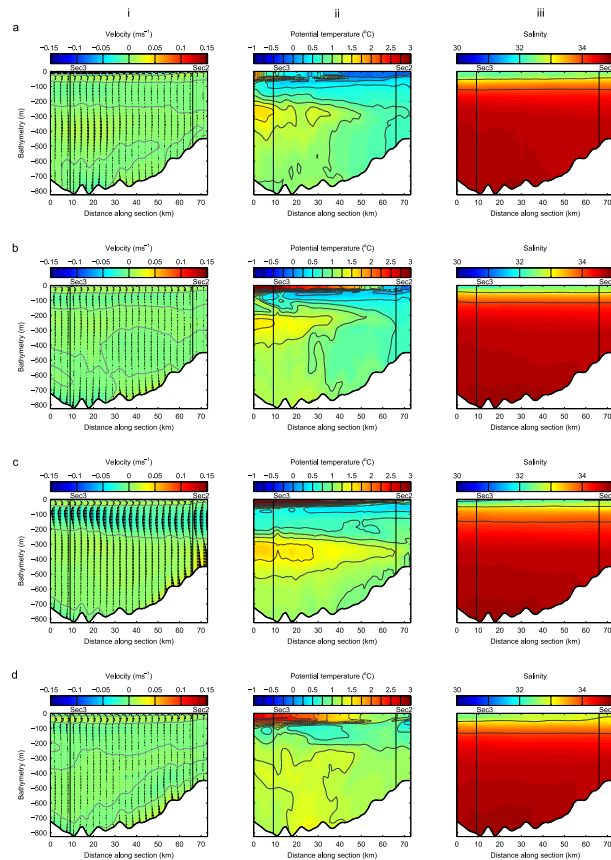


Fig. 6. Longitudinal section (Sect. 1) for experiment CF1-TF1-WF1-RF1. Velocity parallel to Sect. 1 (i), potential temperature (ii) and salinity (iii) for mean of days 0–90 (a), days 91–180 (b), days 181–240 (c) and days 241–365 (d). The fjord mouth is to the left of each plot, and the KG terminus to the right. The FRSZ is not plotted.

Title Page

Abstract

Introduction

Conclusions

References

Tables

Figures

⏪

⏩

◀

▶

Back

Close

Full Screen / Esc

Printer-friendly Version

Interactive Discussion



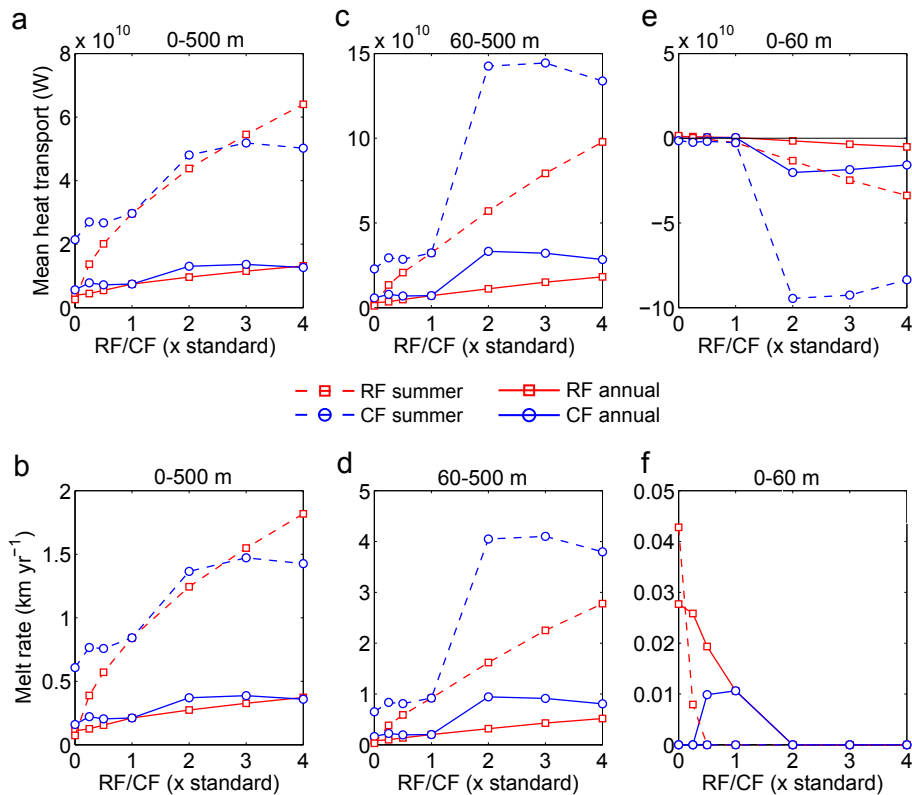


Fig. 7. The effect of varying RF and CF on mean annual and summer along-fjord heat transport (Q) for: **(a)** 0–500 m depth (total); **(c)** 60–500 m depth (intermediate) and; **(e)** 0–60 m depth (shallow). The effect of varying RF and CF on mean annual and summer ice front melt rate for: **(b)** 0–500 m depth (total); **(d)** 60–500 m depth (intermediate) and; **(f)** 0–60 m depth (shallow). Melt rates were calculated from heat transport as described in the main text following Sutherland and Straneo (2012).

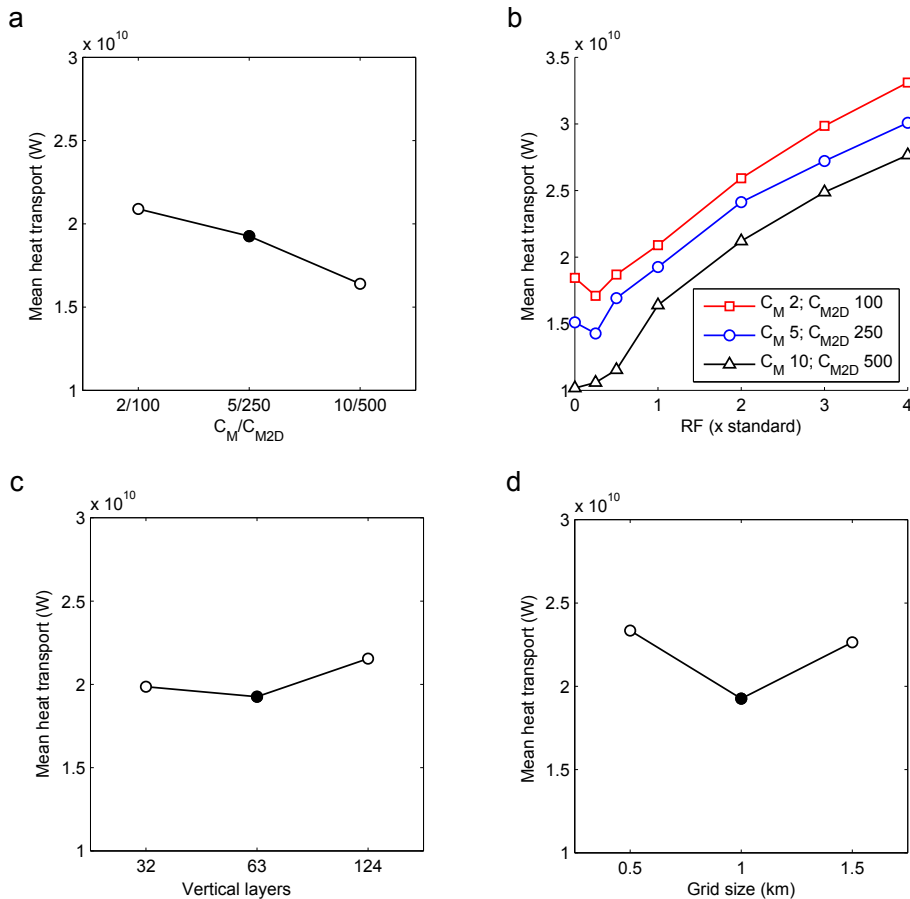


Fig. 8. Sensitivity of along-fjord heat transport to parameter uncertainties. **(a)** and **(b)** 3-D (C_M) and 2-D (C_{M2D}) horizontal viscosity parameters; **(c)** the number of vertical layers in the model; and **(d)** the horizontal model resolution. Solid symbols indicate the standard values for each parameter.

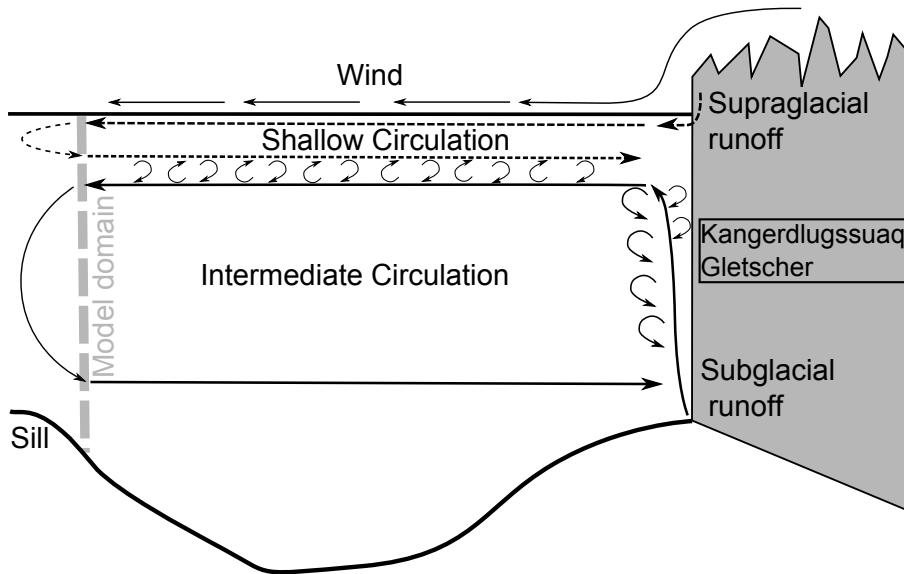


Fig. 9. Schematic of proposed fjord water flow. Simultaneous injection of subglacial and supraglacial runoff, combined with wind stress, produces a four-layer circulation.

Glacier runoff increases ocean heat transport along fjords

A. J. Sole et al.

Title Page

Abstract Introduction

Conclusions References

Tables Figures

◀ ▶

◀ ▶

Back Close

Full Screen / Esc

Printer-friendly Version

Interactive Discussion

